HHS Public Access

Author manuscript

*Methods Enzymol*. Author manuscript; available in PMC 2016 July 23.

Published in final edited form as:

*Methods Enzymol*. 2015 ; 563: 341–361. doi:10.1016/bs.mie.2015.06.030.

# EPR Methods for Biological Cu(II): L-Band CW and NARS

**Brian Bennett** and

Physics Department, 540 N. 15th Street, Marquette University, Milwaukee WI 53233

**Jason Kowalski**

Department of Chemistry, University of Wisconsin-Parkside, Kenosha WI 53144

Brian Bennett: brian.bennett@marquette.edu; Jason Kowalski: kowalski@uwp.edu

## Abstract

Copper has many roles in biology that involve the change of coordination sphere and/or oxidation state of the copper ion. Consequently, the study of copper in heterogeneous environments is an important area in biophysics. EPR is a primary technique for the investigation of paramagnetic copper, which is usually the isolated Cu(II) ion, but sometimes as Cu(II) in different oxidation states of multi-transition ion clusters. The gross geometry of the coordination environment of Cu(II) can often be determined from a simple inspection of the EPR spectrum, recorded in the traditional X-band frequency range (9 – 10 GHz). Identification and quantitation of the coordinating ligand atoms, however, is not so straightforward. In particular, analysis of the superhyperfine structure on the EPR spectrum, to determine the number of coordinated nitrogen atoms, is fraught with difficulty at X-band, despite the observation that the overwhelming number of EPR studies of Cu(II) in the literature have been carried out at X-band. Greater reliability has been demonstrated at S-band (3 – 4 GHz), using the low-field parallel ($g_z$) features. However, analysis relies on clear identification of the outermost superhyperfine line, which has the lowest intensity of all the spectral features. Computer simulations have subsequently indicated that the much more intense perpendicular region of the spectrum can be reliably interpreted at L-band (2 GHz). The present work describes the development of L-band EPR of Cu(II) into a routine method, that is applicable to biological samples.

### Keywords

Copper; electron paramagnetic/spin resonance (EPR, ESR); L-band; nitrogen; coordination

## Background and Introduction

Copper is an element that is essential to life, but is also involved in many diseases and medical conditions (Tisato, Marzano, Porchia, Pellei and Santini 2009). Copper can activate or inhibit enzymes and transporters, promote or suppress redox processes in proteins, promote or inhibit aggregation or fibrillation of proteins, and modulate gene expression (Linder and Hazegh-Azam 1996, Malmstrøm and Leckner 1998, Puig and Thiele 2002, Valentine and Gralla 2002, Perrone, Mothes, Vignes, Mockel, Figueroa, Miquel et al. 2009).

**Dedication.** This chapter is dedicated to Graeme R. Hanson, a valued friend and colleague, who passed away on February 24th, 2015.

Roles of copper in enzymes include electron transfer, oxygen activation, oxygen reduction and denitrification.(Solomon, Heppner, Johnston, Ginsbach, Cirera, Qayyum et al. 2014) The interaction of copper with proteins is suspected to be involved in prion diseases (prion protein, 'PrP', (Wong, Thackray and Bujdoso 2004, Roucou and LeBlanc 2005, Leach, Salman and Hamar 2006, Varela-Nallar, Gonzalez and Inestrosa 2006, Varela-Nallar, Toledo, Chacon and Inestrosa 2006, Millhauser 2007, Nadal, Abdelraheim, Brazier, Rigby, Brown and Viles 2007, Zidar, Pirc, Hodoscek and Bukovec 2008)), Alzheimer's disease (amyloid precursor protein A, (Huang, Cuajungco, Atwood, Hartshorn, Tyndall, Hanson et al. 1999, Maynard, Bush, Masters, Cappai and Li 2005, Bayer, Schafer, Breyhan, Wirths, Treiber and Multhaup 2006, Crouch, White and Bush 2007, Barnham and Bush 2008, Bush 2008, Bush and Tanzi 2008, ********Crouch, Hung, Adlard, Cortes, Lal, Filiz et al. 2009, Drew, Noble, Hanson, Masters and Barnham 2009)), and Parkinson's disease (α-synuclein, (Wright and Brown 2008, Brown 2009)). Cu/Zn superoxide dismutase is a key player in amyotrophic lateral sclerosis (ALS) (Vucic and Kiernan 2009) and interactions of Cu with P-type copper-transporting ATPases are important in Menke's and Wilsons's diseases (de Bie, Muller, Wijmenga and Klomp 2007, La Fontaine and Mercer 2007, Pfeiffer 2007), multidrug resistance and drug transport (Furukawa, Komatsu, Ikeda, Tsujikawa and Akiyama 2008), cancer, and anticancer drug resistance (Kuo, Chen, Song, Savaraj and Ishikawa 2007, Zhang, Li, Yao and Chen 2009). The architecture of serum amyloid A assemblies is Cu-dependent (Wang and Colon 2007) and Cu may play a role in metabolic syndrome (Park, Shin, Kim, Hong and Cho 2010). Formation and stabilization by copper of spherical aggregates of ubiquitin are characteristics of the progression of Alzheimer's, Parkinson's and ALS (Arnesano, Scintilla, Calò, Bonfrate, Ingrosso, Losacco et al. 2009).

Two recent, detailed reviews are highly recommended to the reader with a keen interest in the biophysical study of copper in biological systems.(Antholine, Bennett and Hanson 2011, Solomon et al. 2014) An extensive review of copper in biologically active sites, by Solomon and coworkers (from here on simply referred to as "the Solomon review"),(Solomon et al. 2014) described the electronic structure, electronic structure calculation methods, and relevant spectroscopies (X-ray-based XAS, XES & XMCD; optical and magneto-optical; and EPR, ENDOR and ESEEM), pertaining to Cu(I), Cu(II) and multi-copper sites in copper-containing enzymes. In the latter, consideration was primarily afforded to copper centers in enzymes with roles in electron transfer, oxygen activation, oxygen reduction, and denitrification. Notably absent from the Solomon review were (i) a discussion of multifrequency, particularly low frequency, EPR, and (ii) descriptions of the copper environments in copper chaperones, and in proteins that bind copper and that are associated with neurological diseases, including prions, amyloids and synucleins. The other, in many ways complementary, review described multifrequency EPR of copper in various coordination environments (this review will be referred to as the "ABH review" after the initials of the authors, Antholine, Bennett and Hanson).(Antholine et al. 2011) An introduction to the principles and benefits of multifrequency EPR was first presented with reference to a number of different spin systems, including Cu(II), Mo(V), and Fe(III) and other high-spin systems. There was an emphasis on computer simulation as both a tool for determining spin-Hamiltonian parameters and for learning more fundamentally about the influence of microwave frequency and applied magnetic field on observed transitions. The

application of multifrequency EPR, and particularly low frequency EPR, to Cu(II) was then developed, and the reader is referred to this section of the ABH review in particular as a complement to the present treatment. The ABH review concluded with a survey of experimental studies involving S- (3.4 GHz), C- (4.5 GHz), X- (9 GHz) and Q-band (35 GHz) EPR. Finally, it would be remiss of the present authors not to refer the reader to the section on Cu(II), and additionally to the important appendices K & L, in Pilbrow's seminal work,(Pilbrow 1990) that provides an informative introduction to this field.

Since the publication of the ABH review, the most exciting developments that have occurred in the domain of low frequency EPR of Cu(II) are (i) the development of L-band (2 GHz) as an almost routine technique for the study of Cu(II) in biological material at reasonable amounts (≥ 50 – 100 nmol), and (ii) the development of non-adiabatic rapid scanning (NARS) EPR at 2 GHz and its subsequent application to Cu(II).(Hyde, Bennett, Walter, Millhauser, Sidabras and Antholine 2009, Kittell, Camenisch, Ratke, Sidabras and Hyde 2011, Kowalski and Bennett 2011, Kittell, Hustedt and Hyde 2012, Hyde, Bennett, Kittell, Kowalski and Sidabras 2013, Kittell and Hyde 2015)

## Information from EPR of Cu(II)

EPR spectroscopy has long been used to probe Cu(II) in biological environments, almost since the initial reports in 1945 and 1946 by Zavoisky of the paramagnetic resonance of Cu(II) salts,(Kochelaev and Yablokov 1995). The reasons for performing EPR studies of Cu(II) in biological systems are manifold and include (i) identification of copper; (ii) characterization of geometry of the copper ion(s); (iii) characterization of the ligand sphere; (iv) determination of the number, oxidation states and spin-couplings of copper and/or other transition ions in multi-ion centers or proteins; and (v) spectrokinetic studies of copper active sites or of copper transport and insertion.(Antholine et al. 2011, Bennett and Hill 2011, Solomon et al. 2014). In the case of (i) and (ii), an understanding of the "anatomy" of a Cu(II) EPR signal at a particular frequency is almost always sufficient to unambiguously identify Cu(II) and determine its gross geometry, as the $g$-values and associated $I = {}^3/_2$ hyperfine couplings are well documented and understood from a theoretical perspective. (Pilbrow 1990, Solomon et al. 2014) Briefly, for tetragonal and related square-planar-based geometries, an essentially axial spectrum is expected with $g\| > g\perp > 2$. A highly axial hyperfine interaction with the $I = {}^3/_2$ $^{63}$Cu or $^{65}$Cu nucleus is manifested as a splitting of the $g\|$ resonance into four lines, of which either three or four are typically resolved at X-band, depending on the coordination and its effect on the spin-Hamiltonian parameters;(Peisach and Blumberg 1974) typical spectra are shown in Figure 1. The spectra are a consequence of the nominally $dx^2 - y^2$ ground state paramagnetic orbital (better described as $dx^2 - y^2/dxy$ for lower than ideal symmetry). Severe distortion of tetragonal geometry may, however, introduce mixing of the $dz^2$ orbital into the paramagnetic orbital. This results in a now rhombic **g** tensor, with $g_z > g_y > g_x \approxeq 2$, and $A_z > A_x \gg A_z$, where a four-line pattern is typically only resolved in the $z$ and $x$ orientations (lowest- and highest-field electronic Zeeman resonances, respectively) at X-band. For geometries with a formal $dz^2$ paramagnetic ground state, most notably trigonal bipyramidal in biological systems, then $g\perp > g\| = 2.0$. It is often, then, a reasonably straightforward exercise to determine the gross geometry of a Cu(II) center from the EPR spectrum at X-band. Characterization of copper in multi-ion

clusters is more challenging and, apart from the so-called [$Cu^{1.5}Cu^{1.5}$] $S$ = ½ centers, the information available and the optimum means by which to extract it is largely a function of the interspin interactions and consequent effective zero-field splittings.(Antholine et al. 2011, Solomon et al. 2014)

The most desirable, but often the most challenging, information from EPR is a description of the ligand coordination sphere, particularly in systems that are not amenable to high-resolution structural techniques. In a recent spectrokinetic study, for example, EPR was used to track the change in the equatorial coordination of tetragonal Cu(II) during binding by the *Bacillus subtilis* chaperone involved in Cu site assembly in cytochrome oxidase (BsSCO) from $CuO_4$ in free solution (as $[Cu(H_2O)_6]^{2+}$), via a transient (10 to > 140 ms) $CuO_2N_2$ state, to the final previously characterized and stable $CuN_2S_2$ state.(Bennett et al. 2011) Identification of Cu(II) binding to a quasi-stable preliminary binding site explained how Cu(II) could come to be bound in the destination dithiolate binding site without risk of promoting autoxidation of the sulfhydryls. However, that study also highlighted the challenges of determining the ligand sphere from EPR, particularly at X-band, and relied solely on the Peisach-Blumberg relationships to characterize the $CuO_4$ and $CuO_2N_2$ species (additional support for two coordinated nitrogen atoms in the equilibrium bound $CuN_2S_2$ species was provided by simultaneous computer simulation of the particularly well-resolved X- and Q-band EPR spectra). In their approach, Peisach and Blumberg identified regions on a plot of $A\|$ vs. $g\|$ that correspond to particular combinations of equatorially coordinated sulfur, nitrogen, and oxygen; 2N2S (= $Cu^{II}N_2S_2$), 2N2O, 4S, 4N and 4O (see Figure 2). (Peisach et al. 1974) The correlations are imprecise (imagine, for example, how $CuS_2NO$, $CuO_2S_2$ or $CuSN_2O$ would present) and the 2N2O and 4N regions not only overlap extensively themselves but, over one small area, mutually overlap with 4O! Nevertheless, in many cases the correlations provide some valuable information and have the advantage that the coordination of sulfur or oxygen can be detected in the absence of any reliance on electron-nuclear superhyperfine interaction. The ability of DFT calculations to provide structural models for copper coordination environments based on spin Hamiltonian parameters is becoming increasingly reliable, (Comba, Gahan, Haberhauer, Hanson, Noble, Seibold et al. 2008) although extraction of those parameters from traditional X-band EPR spectra is not as straightforward as is sometimes supposed.(Kowalski et al. 2011) Nitrogen, of course, carries a nuclear spin, $I$ = 1, that provides a three-line multiplet where resolved, so the number of coordinated nitrogens and their superhyperfine coupling constants along the principal electronic Zeeman axes $\mathbf{g}_{xx,\,yy,\,zz}$ are in principle derivable from the EPR spectrum, though this is often not realized in practice due to phenomenological factors that include strain-broadened line widths, overlap of $A(^{14}N)$ with $A\perp(^{63/65}Cu)$, spectral broadening due to the two isotopes of copper present, and overlap of the principal electronic Zeeman resonances with the “overshoot” or “angular anomaly” line(s).(Ovchinnikov and Konstaninov 1978) As was highlighted in a recent study by the present authors, the resolved $^{14}N$ superhyperfine and $^{63/65}Cu$ hyperfine patterns on the perpendicular electronic Zeeman turning point ($g\perp$) are often the only highly resolved features of the spectrum at X-band but lie in a deceptively complex region of the spectrum and do not reliably distinguish between $CuN_3$ and $CuN_4$ equatorial coordination.(Kowalski et al. 2011) Finally, copper also exhibits non-negligible quadrupolar interactions, **I•P•I**, which in principle can provide

information on geometry and symmetry that can, in turn, inform on the ligand sphere. However, quadrupolar interactions can be very difficult to obtain from EPR.(White and Belford 1976, Abrakhmanov and Ivanova 1978, Belford and Duan 1978)

## Strain Broadening, Isotope Broadening, and the Overshoot Line

Strain broadening is a term used to denote the frequency-dependent broadening of the line width, Δ, where, here, $\Delta = \sqrt{[\Delta^2_{\text{intrinsic}} + (m_I\sigma A)^2 + [(h\nu/g^2\beta_e)\sigma g]^2 - 2\varepsilon m_I(h\nu/g^2\beta_e)\sigma g\sigma A}$ for the $m_I$ manifolds of the $I = {}^3/_2$ hyperfine-split resonances of a tetragonal system (Froncisz, Scholes, Hyde, Wei, King, Shaw et al. 1979, Froncisz, Sarna and Hyde 1980, Hyde and Froncisz 1982). In this expression, $\sigma g$ and $\sigma A$ represent distributions ('strains') in the principal values of $g$ and $A$ due to microheterogeneity of the electronic structures of the Cu(II) ions in the sample. This may be due, for example, to the immobilization of low-lying conformational/vibrational sub-states upon freezing of a solution in liquid nitrogen. Model strain-dependent line widths (Hyde, Antholine, Froncisz and Basosi 1986) for $m_I$ manifolds of the $g\|$ resonance of Cu(II) as a function of microwave frequency are shown graphically in Figure 3. At frequencies approaching X-band, and at all frequencies above, it can be seen from Figure 3 that the line width of each resonance increases linearly and rapidly with frequency, as the $g$-strain-dependent field envelope of the resonant line, $\Delta B_g \propto \nu/\sigma g$, (i.e. $\propto \nu$) whereas its hyperfine-dependent analog $\Delta B_A$ is field- (frequency) independent and rapidly becomes insignificant at higher frequencies. At lower frequencies, however, where $\Delta B_g \approxeq |\Delta B_A|$, then, for two of the four $I = {}^3/_2$ lines, the term $-2\varepsilon m_I(h\nu/g^2\beta_e)\sigma g\sigma A$ must adopt a negative value. Depending on the values of the strains themselves and the $g$-strain-$A$-strain coupling, ε, the $g$- and $A$-strains consequently more-or-less cancel each other in a frequency-dependent manner, and a frequency will exist for each of the two lines at which optimal *strain narrowing* will be observed. This phenomenon can be exploited using multifrequency EPR to optimize the extraction of the number of equatorially coordinated nitrogen atoms, a goal often of value, *e.g.* in determining the order of binding, or partition of, copper in multi-site proteins.(Chattopadhyay, Walter, Newell, Jackson, Aronoff-Spencer, Peisach et al. 2005, Hyde et al. 2009, Kowalski et al. 2011) (Note that while for some systems, *e.g.* thiolate coordinated Cu(II) or Cu(II)-substituted heme proteins, significant strain narrowing of the lowest-field $m_I = +{}^3/_2$ manifold may be observed between 3.5 and 9 GHz,(Hyde et al. 1986, Pasenkiewicz-Gierula, Antholine, Subczynski, Baffa, Hyde and Petering 1987) $g$-strain broadening precludes superhyperfine resolution of this manifold for most biological Cu(II) species).

A second phenomenon of specific significance to copper is isotope broadening. Naturally abundant copper consists of ≈ 69 % $^{63}$Cu with $g_n = 1.484$ and $Q/e = -220$ b (1 b = $10^{-28}$ m$^2$), and ≈ 31 % $^{65}$Cu with $g_n = 1.588$ and $Q/e = -204$ b. There are three consequences of this isotopic distribution. The quadrupole moment ratio is ≈ 1.08, and the magnitude of the quadrupolar coupling itself is generally ≤ 15 MHz, *i.e.* ≤ 5 G, so any broadening due to the distinct quadrupole moments of $^{63}$Cu and $^{65}$Cu is limited to < 0.5 G and the isotopic dependence can usually be neglected. Similarly, while the field- (and frequency-) dependent nuclear Zeeman interaction is significant for Cu(II), ≈ 2 G at X-band, the difference in value between the two isotopes is only ≈ 0.14 G at X-band and, again, this difference can be neglected for X-band and lower frequencies in almost all cases. In contrast, the nuclear

magnetic moment ratio of ≈ 0.93 is significant, as it applies to much larger absolute values. For a typical $A\|(^{63}Cu)$ of 185 G, the corresponding value for $A\|(^{65}Cu)$ is 198 G, *i.e.* $\Delta A\|$ ($^{65}Cu$ - $^{63}Cu$) ≈ 13 G. A typical $^{14}N$ superhyperfine coupling is also ≈ 13 G. The relative displacements of the $m_I = +^3/_2$, +½, − ½ and − ½ manifolds due to $^{65}Cu$ from those due to $^{63}Cu$ are −19.5, −6,5, +6.5 and +19.5 G. Consequently, for each $A\|$(Cu) manifold, the $^{14}N$ superhyperfine patterns will experience "destructive interference", with the broadening of the outer lines of these patterns being particularly severe as the more intense of the $^{65}Cu$ lines are out of phase with the less intense of the $^{63}Cu$ lines and the natural isotopic abundance ensures almost complete cancellation. The intensities of the superhyperfine lines for the inner ±½ patterns will no longer obey the symmetrical binomial distribution and a shoulder on the outer line will be expected due to the higher $g_n$, lower isotopic fraction $^{65}Cu$ contribution. The outer $\pm^3/_2$ patterns will be more distorted, with an isolated "extra" $^{65}Cu$ line outside the dominant $^{63}Cu$ pattern. In practice, the expected loss of resolution, particularly on the lower-field (outer) side of the resolved +½ pattern, is indeed observed at frequencies where superhyperfine structure is resolved from samples containing naturally abundant isotopes of copper (Figure 4). The effect of the isotopic constitution of naturally abundant copper on the observed perpendicular copper hyperfine splitting is much smaller than for the parallel splitting. $A\perp$(Cu) values actually exhibit some rhombicity ($A_x \neq A_y$) and vary much more than the essentially isotropic but roughly similar values for coordinated-nitrogen superhyperfine, with values of $A_{x/y}$(Cu) from 5 to 20 × $10^{-4}$ $cm^{-1}$ reported. (Ammeter, Rist and Günthard 1972, Hyde et al. 2009, Kowalski et al. 2011, Hyde et al. 2013) Taking an arbitrary value of 15 G for $A\perp(^{63}Cu)$, then the value of $A\perp(^{65}Cu)$ is expected to be ≈ 16.1 G; the resulting broadening of ≈ 1 G is tolerable.(Hyde et al. 2013)

Finally, any discussion of EPR of Cu(II) would be incomplete without a discussion of the "overshoot" or "angular anomaly" that is a feature of Cu(II) EPR spectra.(Ovchinnikov et al. 1978) The overshoot line arises from the differential change in resonant field due to the orientation-dependent changes in the anisotropic **g** and **A**(Cu) tensors; phenomenologically, the hyperfine pattern expands "faster" than the *g*-value decreases, as the molecular orientation transitions from $x\|\mathbf{B}$ or $y\|\mathbf{B}$ to $z\|\mathbf{B}$, as sketched in Figure 5. At X-band (Figure 5, top), the highest resonant field "overshoots" that corresponding to the highest-field hyperfine resonance of either of the principal electronic Zeeman resonances (hence the name) and manifests itself as an additional resonance in the powder spectrum that is easily mistaken for evidence of a rhombic **g** tensor with three distinct principal values (see Figure 1, top). At lower frequencies, either one or two overshoot lines may appear within the field envelope of the spectrum (see Figure 5, bottom), whereas simulations (Figure 6) indicate that the overshoot line contributes to the highest field resonance in spectra recorded at frequencies up to 95 GHz (*g*-strain usually precludes clear experimental demonstration of this effect at frequencies beyond X-band, though it has been demonstrated at 35 GHz). (Bennett et al. 2011) The primary consequences of the overlap of the overshoot line and the $g\perp$ resonance are an inability to reliably count the number of lines in the patterns due to magnetic copper and nitrogen nuclei, and difficulty in extraction of spin Hamiltonian parameters even by computer simulation, particularly where non-coincidence of **g** and **A** is significant. The combination of strain-broadening of the parallel resonances and the overlap of the overshoot line with the perpendicular resonances render X-band a frequency that is

particularly unsuited for the high-resolution study of Cu(II)! It is with some sense of irony, then, that the reader may care to reflect on the fact that the overwhelming majority of EPR of Cu(II) is recorded at X-band, as evidenced by the observation that, of the 70 experimental EPR spectra reproduced in the Solomon review, 68 were recorded at X-band (the remaining two were at Q-band, 35 GHz).(Solomon et al. 2014)

## Low Frequency EPR of Cu(II)

Multifrequency EPR, particularly EPR at < 9.5 GHz, has long been employed to better characterize the (equatorial) ligand coordination of Cu(II),(Rakhit, Antholine, Froncisz, Hyde, Pilbrow, Sinclair et al. 1985, Kroneck, Antholine, Riester and Zumft 1988, Antholine, Kastrau, Steffens, Buse, Zumft and Kroneck 1992, Neese, Zumft, Antholine and Kroneck 1996, Aronoff-Spencer, Burns, Avdievich, Gerfen, Peisach, Antholine et al. 2000, Burns, Aronoff-Spencer, Dunham, Lario, Avdievich, Antholine et al. 2002, Burns, Aronoff-Spencer, Legname, Prusiner, Antholine, Gerfen et al. 2003, Chattopadhyay et al. 2005) and the rationale for a truly multifrequency approach to EPR of Cu(II) is presented in the ABH review, in the wider context of multifrequency EPR in general.(Antholine et al. 2011) The genesis of the rational application of low frequency EPR to Cu(II) is to be found in the treatment of strains by Froncisz and Hyde.(Froncisz et al. 1979, Froncisz and Hyde 1980, Hyde et al. 1982) This analysis and its experimental verification showed that in the region 1 – 4 GHz, one of the two lower-field parallel resonances are optimally resolved due to strain-narrowing. The contemporaneous development of the loop-gap resonator (LGR) was also crucial to the adoption of low-frequency EPR for the high-resolution EPR study of Cu(II). (Froncisz and Hyde 1982, Hyde and Froncisz 1986) The size of traditional cavity resonators for EPR scale essentially as the wavelength of the microwave radiation, λ, so the volume scales as the cube of λ, making the active volume of a 2 GHz resonator some 75 × larger than a traditional X-band cavity, and requiring some 20 mL of sample, prohibitive for many biological systems. The development of the LGR facilitated the use of much smaller samples, and fuelled the highly productive application of S-band (3.4 GHz) EPR to biological and inorganic copper systems by Antholine and co-workers.(Antholine et al. 2011) More recently, Hyde, Sidabras and coworkers developed, first, a one-loop-one-gap 0.5 mL LGR for EPR at 1.9 GHz, (Hyde et al. 2009) and subsequently, a 0.25 mL two-loop-one-gap resonator with improved microwave shielding and superior mechanical and temperature stability.(Kowalski et al. 2011, Hyde et al. 2013) These structures allowed for the study of limited biological samples such as prion protein, and are shown along with the corresponding cavity resonator in Figure 7.

Another development that spurred the adoption of low-frequency EPR was improved, user-friendly computer simulations.(Hanson, Gates, Noble, Mitchell, Benson, Griffin et al. 2003, Hanson, Gates, Noble, Griffin, Mitchell and Benson 2004) Indeed, the adoption of 2 GHz as the frequency of choice for the study of Cu(II) was based upon computer simulations of the EPR absorption envelope (Figure 8). As is clear from the figure, as the microwave frequency is lowered from X-band (9.5 GHz), an overshoot line emerges from the complex high-field region of the higher frequency spectra, until it is optimally resolved from other spectra features at 2 GHz. At yet lower frequencies, the energy levels between which the EPR transitions occur become complex themselves (Figure 9) and the spectra at 1 GHz

reflect this complexity. At 2 GHz, though, the overshoot line is highly resolved and can now be viewed as a source of information, rather than a complicating feature. The “anatomy” of a typical L-band spectrum at 1.85 GHz is illustrated in Figure 10. Here, three of the hyperfine manifolds of the parallel electronic Zeeman resonance are resolved, PA, PB & PD, with $^{14}$N superhyperfine structure observed on the PB ($m_I$ = +½) line with $A\|(4 \times {}^{14}\mathrm{N})$ = 12.3 G (the superhyperfine lines are labeled PB1 to PB7 in the lower tile of the figure). The EPR absorption manifolds are shown below the spectrum, calculated without the $^{14}$N superhyperfine contribution. The central “perpendicular” region of the spectrum is composed of two regions. One exhibits superhyperfine structure with a splitting equal to the value $A\perp(^{14}\mathrm{N})$ = 14.4 G (labeled A1 to A6). This region corresponds to the genuine perpendicular electronic Zeeman resonance, $g\perp$. The adjacent region (B1 – B6) exhibits a splitting of 13.1 G, intermediate between the values for $A\|$ and $A\perp$, and corresponds to the overshoot line of indeterminate orientation (it can, in fact, be estimated by “roadmap” simulations). The center of the pattern due to the overshoot line can be determined from the EPR absorption spectrum, where it dominates the overlapping but much less intense perpendicular feature of the $m_I = -3/2$ manifold, and analysis (usually by simulation) of the high-field side of this feature provides the number of equatorially-coordinated nitrogen atoms. This method was successfully used to determine the coordination of copper bound to a prion protein fragment that had defied characterization by X- and S-band EPR, and electron spin-echo envelope-modulation (ESEEM) spectroscopy.(Chattopadhyay et al. 2005, Hyde et al. 2009) The characterization of other prion-bound species of copper was subsequently and similarly carried out, with additional verification of the number of coordinated nitrogen atoms being provided by analyses of the parities of the Fourier transforms of the EPR spectra.(Pasenkiewicz-Gierula, Froncisz, Basosi, Antholine and Hyde 1987, Della Lunga, Pogni and Basosi 1995, Kowalski et al. 2011) This latter, often neglected, method discriminates between odd and even numbers of magnetic nuclei that contribute essentially equally to a superhyperfine pattern, and is particularly useful for discriminating 3 versus 4 coordinated nitrogens where the data quality does not allow definitive identification of the weakest outer superhyperfine line.

## Non-Adiabatic Rapid Sweep (NARS) EPR Spectroscopy

NARS is a term used to describe a rapid scanning methodology in which the magnetic field is scanned sufficiently rapidly through the spectrum to significantly abate 1/*f* noise but sufficiently slowly so as to maintain the system in thermal equilibrium.(Kittell et al. 2011) Phase-sensitive detection is dispensed with and the spectral display is that of a pure absorption spectrum with about 4 × the signal-to-noise ratio of conventional EPR under otherwise equivalent conditions with no attendant modulation broadening or distortion. The technique was developed for the purpose of detecting small line-broadening due to dipolar coupling between two spin labels separated by up to 40 Å, and low frequency (1 – 2 GHz) was employed in order to collapse the **g** tensor at the low resonant fields and, hence, increase the distance limit of the method.(Kittell et al. 2012) The enhanced signal to noise, the flexibility of multiple data processing options on the same dataset, the absence of field modulation artifacts, and the development at L-band were seen as attractive for the study of Cu(II), and NARS was subsequently adapted for that purpose by the present authors and co-

workers.(Hyde et al. 2013) The major adaptation arose because the field envelope of the Cu(II) spectrum is far too wide to be scanned at audio frequencies using conventional electromagnetic coils. The solution was to scan the spectrum in segments and concatenate the fragments (shown schematically in Figure 11). The fragment size was deliberately chosen so as not to correspond to the expected width or separation of any features in the spectrum. Artifacts that occurred during the automated concatenation of the fragments were then isolated in the Fourier transform and edited prior to reverse transformation back to the absorption spectrum. This proved to be highly effective. The goal was to use the NARS method to characterize nitrogen coordinated to copper. However, the absorption display was not ideal for displaying the superhyperfine pattern due to the intense underlying body of the absorption spectrum, and various methods of transforming the dataset to a derivative-like display were evaluated. The most successful one appeared to be a simple moving difference algorithm (“MDIFF”), that had not apparently been employed previously in the context of EPR spectroscopy, but that was an effective way of preferentially increasing the intensity of narrow features relative to broad ones.(Hyde et al. 2013) The MDIFF algorithm can equally well be applied to experimental and simulated absorption data, facilitating the use of simulations for spectral analysis. Further, the MDIFF amplitude (analogous to the field modulation amplitude) can be arbitrarily varied, and the amplitude at which the spectral lines begin to lose intensity through broadening provided a sensitive and reproducible method for determining line widths. Finally, it was found that the MDIFF algorithm was an effective and selective low-frequency filter, much more so than mere averaging, that was ideally suited to EPR spectra that contain narrow features and that require stringent conditions for high-resolution, but that overlap broad, gross features with wide field envelopes. The technique is thus eminently suited to low-frequency EPR of copper, though many other applications can be imagined.

## Literature cited


Abrakhmanov RS, Ivanova TA. Possible use of low-frequency ESR to estmate the quadrupole coupling constant in copperII complexes. J Struct Chem. 1978; 19:145–148.

Ammeter J, Rist GH, Günthard HA. Influence of the host lattice upon EPR coupling parameters and d-d transitions of planar copper (II) complexes. J Chem Phys. 1972; 57:3852–3866.

Antholine, WE.; Bennett, B.; Hanson, GR. Copper Coordination Environments. In: Misra, SK., editor. Multifrequency Electron Paramagnetic Resonance. Berlin: Wiley-VCH; 2011. p. 647-715.

Antholine WE, Kastrau DHW, Steffens GCM, Buse G, Zumft WG, Kroneck PMH. A comparative EPR investigation of the multicopper proteins nitrous oxide reductase and cytochrome c oxidase. Eur J Biochem. 1992; 209:875–881. [PubMed: 1330560]

Arnesano F, Scintilla S, Calò V, Bonfrate E, Ingrosso C, Losacco M, Pellegrino T, Rizzarelli E, Natile G. Copper-triggered aggregation of ubiquitin. PLoS One. 2009; 4:e7052. [PubMed: 19756145]

Aronoff-Spencer E, Burns CS, Avdievich NI, Gerfen GJ, Peisach J, Antholine WE, Ball HL, Cohen FE, Prusiner SB, Millhauser GL. Identification of the Cu2+ binding sites in the N-terminal domain of the prion protein by EPR and CD spectroscopy. Biochemistry. 2000; 39(45):13760–13771. [PubMed: 11076515]

Barnham KJ, Bush AI. Metals in Alzheimer’s and Parkinson’s diseases. Curr Opin Chem Biol. 2008; 12(2):222–228. [PubMed: 18342639]

Bayer TA, Schafer S, Breyhan H, Wirths O, Treiber C, Multhaup G. A vicious circle: role of oxidative stress, intraneuronal Abeta and Cu in Alzheimer’s disease. Clin Neuropathol. 2006; 25(4):163–171. [PubMed: 16866297]

Belford RL, Duan DC. Determination of nuclear quadrupolar coupling by simulation of EPR spectra of frozen solutions. J Magn Reson. 1978; 29:293–307.

Bennett B, Hill BC. Avoiding premature oxidation during the binding of Cu(II) to a dithiolate site in BsSCO. A rapid freeze-quench EPR study. FEBS Lett. 201110.1016/j.febslet.2011.1002.1014

Brown DR. Metal binding to alpha-synuclein peptides and its contribution to toxicity. Biochem Biophys Res Commun. 2009; 380:377–381. [PubMed: 19250637]

Burns CS, Aronoff-Spencer E, Dunham CM, Lario P, Avdievich NI, Antholine WE, Olmstead MM, Vrielink A, Gerfen GJ, Peisach J, Scott WG, Millhauser GL. Molecular features of the copper binding sites in the octarepeat domain of the prion protein. Biochemistry. 2002; 41(12):3991–4001. [PubMed: 11900542]

Burns CS, Aronoff-Spencer E, Legname G, Prusiner SB, Antholine WE, Gerfen GJ, Peisach J, Millhauser GL. Copper coordination in the full-length, recombinant prion protein. Biochemistry. 2003; 42(22):6794–6803. [PubMed: 12779334]

Bush AI. Drug development based on the metals hypothesis of Alzheimer's disease. J Alzheimers Dis. 2008; 15(2):223–240. [PubMed: 18953111]

Bush AI, Tanzi RE. Therapeutics for Alzheimer's disease based on the metal hypothesis. Neurotherapeutics. 2008; 5(3):421–432. [PubMed: 18625454]

Chattopadhyay M, Walter ED, Newell DJ, Jackson PJ, Aronoff-Spencer E, Peisach J, Gerfen GJ, Bennett B, Antholine WE, Millhauser GL. The octarepeat domain of the prion protein binds Cu(II) with three distinct coordination modes at pH.7.4. J Am Chem Soc. 2005; 127:12647–12656. [PubMed: 16144413]

Comba P, Gahan LR, Haberhauer G, Hanson GR, Noble CJ, Seibold B, van den Brenk AL. Copper(II) Coordination Chemistry of Westiellamide and Its Imidazole, Oxazole, and Thiazole Analogues. Chem Eur J. 2008; 14:4394–4403.

Crouch PJ, Hung LW, Adlard PA, Cortes M, Lal V, Filiz G, Perez KA, Nurjono M, Caragounis A, Du T, Laughton K, Volitakis I, Bush AI, Li QX, Masters CL, Cappai R, Cherny RA, Donnelly PS, White AR, Barnham KJ. Increasing Cu bioavailability inhibits Abeta oligomers and tau phosphorylation. Proc Natl Acad Sci U S A. 2009; 106(2):381–386. [PubMed: 19122148]

Crouch PJ, White AR, Bush AI. The modulation of metal bio-availability as a therapeutic strategy for the treatment of Alzheimer's disease. Febs J. 2007; 274(15):3775–3783. [PubMed: 17617225]

de Bie P, Muller P, Wijmenga C, Klomp LW. Molecular pathogenesis of Wilson and Menkes disease: correlation of mutations with molecular defects and disease phenotypes. J Med Genet. 2007; 44:673–688. [PubMed: 17717039]

Della Lunga G, Pogni R, Basosi R. Discrimination of Copper-Nitrogen Ligand Coordination by Fourier Analysis of EPR Spectra in Mobile Phase. J Magn Reson A. 1995; 114:174–178.

Drew SC, Noble CJ, Hanson GR, Masters CL, Barnham KJ. Pleomorphic Cu2+ coordination of Alzheimer's amyloid-$\beta$ peptide. J Am Chem Soc. 2009; 131:1195–1207. [PubMed: 19119811]

Froncisz W, Hyde JS. Broadening by strains of lines in the g-parallel region of Cu2+ EPR spectra. J Chem Phys. 1980; 73:3123–3131.

Froncisz W, Hyde JS. The Loop-Gap Resonator: A New Microwave Lumped Circuit ESR Sample Structure. J Magn Reson. 1982; 47:515–521.

Froncisz W, Sarna T, Hyde JS. Cu2+ probe of metal-ion binding sites in melanin using electron paramagnetic resonance spectroscopy. I. Synthetic melanins. Arch Biochem Biophys. 1980; 202(1):289–303. [PubMed: 6249219]

Froncisz W, Scholes CP, Hyde JS, Wei YH, King TE, Shaw RW, Beinert H. Hyperfine structure resolved by 2 to 4 GHz EPR of cytochrome c oxidase. J Biol Chem. 1979; 254(16):7482–7484. [PubMed: 224030]

Furukawa T, Komatsu M, Ikeda R, Tsujikawa K, Akiyama S. Copper transport systems are involved in multidrug resistance and drug transport. Curr Med Chem. 2008; 15:3266–3278.

Hanson GR, Gates KE, Noble CJ, Griffin M, Mitchell A, Benson S. XSophe-Sophe-XeprView: A Computer Simulation Suite (v.1.1.3) for the Analysis of Continuous Wave EPR Spectra. J Inorg Biochem. 2004; 98:903–916. [PubMed: 15134936]

Hanson, GR.; Gates, KE.; Noble, CJ.; Mitchell, A.; Benson, S.; Griffin, M.; Burrage, K. XSophe-Sophe-XeprView: A computer simulation software suite for the analysis of continuous wave EPR

spectra. In: Shiotani, M.; Lund, A., editors. EPR of Free Radicals in Solids: Trends in Methods and Applications. Dordrecht: Kluwer Press; 2003. p. 197-237.

Huang X, Cuajungco MP, Atwood CS, Hartshorn MA, Tyndall JD, Hanson GR, Stokes KC, Leopold M, Multhaup G, Goldstein LE, Scarpa RC, Saunders AJ, Lim J, Moir RD, Glabe C, Bowden EF, Masters CL, Fairlie DP, Tanzi RE, Bush AI. Cu(II) potentiation of alzheimer Abeta neurotoxicity. Correlation with cell-free hydrogen peroxide production and metal reduction. J Biol Chem. 1999; 274(52):37111–37116. [PubMed: 10601271]

Hyde, JS.; Antholine, WE.; Froncisz, W.; Basosi, R. EPR determination of the number of nitrogens coordinated to Cu in square-planar complexes. In: Nicolai, N.; Valensin, G., editors. Advanced Magnetic Resonance Techniques in Systems of High Molecular Complexity. Boston: Birkhauser; 1986. p. 363-384.

Hyde JS, Bennett B, Kittell AW, Kowalski JM, Sidabras JW. Moving difference (MDIFF) non-adiabatic rapid sweep (NARS) EPR of copper(II). J Magn Reson. 2013; 236:15–25. [PubMed: 24036469]

Hyde JS, Bennett B, Walter ED, Millhauser GL, Sidabras GW, Antholine WE. EPR of Cu prion protein constructs at 2.0 GHz using the g-perpendicular region to characterize nitrogen ligation. Biophys J. 2009; 96:3354–3362. [PubMed: 19383478]

Hyde JS, Froncisz W. The role of microwave frequency in EPR spectroscopy of copper complexes. Annu Rev Biophys Bioeng. 1982; 11:391–417. [PubMed: 6285804]

Hyde JS, Froncisz W. Loop Gap Resonators. Specialist Periodical Reports of the Royal Society of Chemistry. 1986; 10:175–184.

Kittell AW, Camenisch TG, Ratke JJ, Sidabras JW, Hyde JS. Detection of undistorted continuous wave (CW) electron paramagnetic resonance (EPR) spectra with non-adiabatic rapid sweep (NARS) of the magnetic field. J Magn Reson. 2011; 211:228–233. [PubMed: 21741868]

Kittell AW, Hustedt EJ, Hyde JS. Inter-spin distance determination using L-band (1–2 GHz) non-adiabatic rapid sweep electron paramagnetic resonance (NARS EPR). J Magn Reson. 2012; 221:51–56. [PubMed: 22750251]

Kittell AW, Hyde JS. Spin-label CW microwave power saturation and rapid passage with triangular non-adiabatic rapid sweep (NARS) and adiabatic rapid passage (ARP) EPR spectroscopy. J Magn Reson. 2015; 255:68–76. [PubMed: 25917132]

Kochelaev, BI.; Yablokov, YV. The Beginning of Paramagnetic Resonance. Singapore: World Scientific; 1995.

Kowalski JM, Bennett B. Spin Hamiltonian Parameters for Cu(II)-Prion Peptide Complexes from L-band Electron Paramagnetic Resonance Spectroscopy. J Am Chem Soc. 2011; 133:1814–1823. [PubMed: 21265507]

Kroneck PMH, Antholine WA, Riester J, Zumft WG. The cupric site in nitrous oxide reductase contains a mixed-valence [Cu(II), Cu(I)] binuclear center: a multi-frequencey electron paramagnetic resonance investigation. FEBS Lett. 1988; 242:70–74. [PubMed: 2849565]

Kuo MT, Chen HH, Song IS, Savaraj N, Ishikawa T. The roles of copper transporters in cisplatin resistance. Cancer Metastasis Rev. 2007; 26:71–83. [PubMed: 17318448]

La Fontaine S, Mercer JF. Trafficking of the copper-ATPases, ATP7A and ATP7B: role in copper homeostasis. Arch Biochem Biophys. 2007; 463:149–167. [PubMed: 17531189]

Leach SP, Salman MD, Hamar D. Trace elements and prion diseases: a review of the interactions of copper, manganese and zinc with the prion protein. Anim Health Res Rev. 2006; 7(1–2):97–105. [PubMed: 17389057]

Linder MC, Hazegh-Azam M. Copper biochemistry and molecular biology. Am J Clin Nutr. 1996; 63:797S–811S. [PubMed: 8615367]

Malmstrøm BG, Leckner J. The chemical biology of copper. Curr Opin Chem Biol. 1998; 2:286–292. [PubMed: 9667936]

Maynard CJ, Bush AI, Masters CL, Cappai R, Li QX. Metals and amyloid-beta in Alzheimer's disease. Int J Exp Pathol. 2005; 86(3):147–159. [PubMed: 15910549]

Millhauser GL. Copper and the prion protein: methods, structures, function, and disease. Ann Rev Phys Chem. 2007; 58:299–320. [PubMed: 17076634]

Nadal RC, Abdelraheim SR, Brazier MW, Rigby SE, Brown DR, Viles JH. Prion protein does not redox-silence Cu2+, but is a sacrificial quencher of hydroxyl radicals. Free Radic Biol Med. 2007; 42(1):79–89. [PubMed: 17157195]

Neese F, Zumft WG, Antholine WE, Kroneck PMH. The purple mixed valence CuA center in nitrous oxide reductase: EPR of the copper-63 and copper-65, and both copper-65 and [15N]Histidine-enriched enzyme and a molecular orbital interpretation. J Am Chem Soc. 1996; 118:8692–8699.

Ovchinnikov IV, Konstaninov VN. Extra absorption peaks in EPR spectra of systems with anisotropic g-tensor and hyperfine structure in powders and glasses. J Magn Reson. 1978; 32:179–190.

Park KH, Shin DG, Kim JR, Hong JH, Cho KH. The functional and compositional properties of lipoproteins are altered in patients with metabolic syndrome with increased cholesteryl ester transfer protein activity. Int J Mol Med. 2010; 25:129–136. [PubMed: 19956911]

Pasenkiewicz-Gierula M, Antholine WE, Subczynski WK, Baffa O, Hyde JS, Petering DH. Assessment of the ESR spectra of CuKTSM2. Inorg Chem. 1987; 26:3945–3949.

Pasenkiewicz-Gierula M, Froncisz W, Basosi R, Antholine WE, Hyde JS. Multifrequency ESR with Fourier analysis of CuII(His)n (His = histidine). 2. Mobile phase. Inorg Chem. 1987; 26:801–805.

Peisach J, Blumberg WE. Structural Implications Derived from the Analysis of Electron Paramagnetic Resonance Spectra of Natural and Artificial Copper Proteins. Arch Biochem Biophys. 1974; 165:691–708. [PubMed: 4374138]

Perrone L, Mothes E, Vignes M, Mockel A, Figueroa C, Miquel MC, Maddelein ML, Faller P. Copper Transfer from Cu-Abeta to Human Serum Albumin Inhibits Aggregation, Radical Production and Reduces Abeta Toxicity. Chembiochem. 2009; 11:110–118. [PubMed: 19937895]

Pfeiffer RF. Wilson's Disease. Semin Neurol. 2007; 27:123–132. [PubMed: 17390257]

Pilbrow, JR. Transition Ion Electron Paramagnetic Resonance. Oxford University Press; Oxford U.K: 1990.

Puig S, Thiele DJ. Molecular mechanisms of copper uptake and distriibution. Curr Opin Chem Biol. 2002; 6:171–180. [PubMed: 12039001]

Rakhit G, Antholine WE, Froncisz W, Hyde JS, Pilbrow JR, Sinclair GR, Sarkar B. Direct evidence of nitrogen coupling in the copper(II) complex of bovine serum albumin by S-band electron spin resonance technique. J Inorg Biochem. 1985; 25(3):217–224. [PubMed: 2999331]

Roucou X, LeBlanc AC. Cellular prion protein neuroprotective function: implications in prion diseases. J Mol Med. 2005; 83:3–11. [PubMed: 15645198]

Solomon EI, Heppner DE, Johnston EM, Ginsbach JW, Cirera J, Qayyum M, Kieber-Emmons MT, Kjaergaard CH, Hadt RG, Tian L. Copper active sites in biology. Chem Rev. 2014; 114(7):3659–3853. [PubMed: 24588098]

Tisato F, Marzano C, Porchia M, Pellei M, Santini C. Copper in diseases and treatments, and copper-based anticancer strategies. Anticancer Agents Med Chem. 2009; 9:185–211. [PubMed: 19199864]

Valentine, JS.; Gralla, EB., editors. Advances in Protein Chemistry. New York: Academic Press; 2002. Copper-Containing Molecules.

Varela-Nallar L, Gonzalez A, Inestrosa NC. Role of copper in prion diseases: deleterious or beneficial? Curr Pharm Des. 2006; 12(20):2587–2595. [PubMed: 16842180]

Varela-Nallar L, Toledo EM, Chacon MA, Inestrosa NC. The functional links between prion protein and copper. Biol Res. 2006; 39(1):39–44. [PubMed: 16629163]

Vucic S, Kiernan MC. Pathophysiology of neurodegeneration in familial amyotrophic lateral sclerosis. Curr Mol Med. 2009; 9:255–272. [PubMed: 19355908]

Wang L, Colon W. Effect of zinc, copper, and calcium on the structure and stability of serum amyloid A. Biochemistry. 2007; 46:5562–5569. [PubMed: 17425332]

White LK, Belford RL. Quadrupole coupling constants of square-planar copper(II)-sulfur complexes from single-crystal electron paramagnetic resonance spectroscopy. J Am Chem Soc. 1976; 98:4428–4438.

Wong E, Thackray AM, Bujdoso R. Copper induces increased beta-sheet content in the scrapie-susceptible ovine prion protein PrPVRQ compared with the resistant allelic variant PrPARR. Biochem J. 2004; 380(Pt 1):273–282. [PubMed: 14969585]

Wright JA, Brown DR. Alpha-synuclein and its role in metal binding: relevance to Parkinson's disease. J Neuroci Res. 2008; 88:496–503.

Zhang Y, Li M, Yao Q, Chen C. Roles and mechanisms of copper transporting ATPases in cancer pathogenesis. Med Sci Monit. 2009; 15:RA1–5. [PubMed: 19114980]

Zidar J, Pirc ET, Hodoscek M, Bukovec P. Copper(II) ion binding to cellular prion protein. J Chem Inf Model. 2008; 48(2):283–287. [PubMed: 18247504]

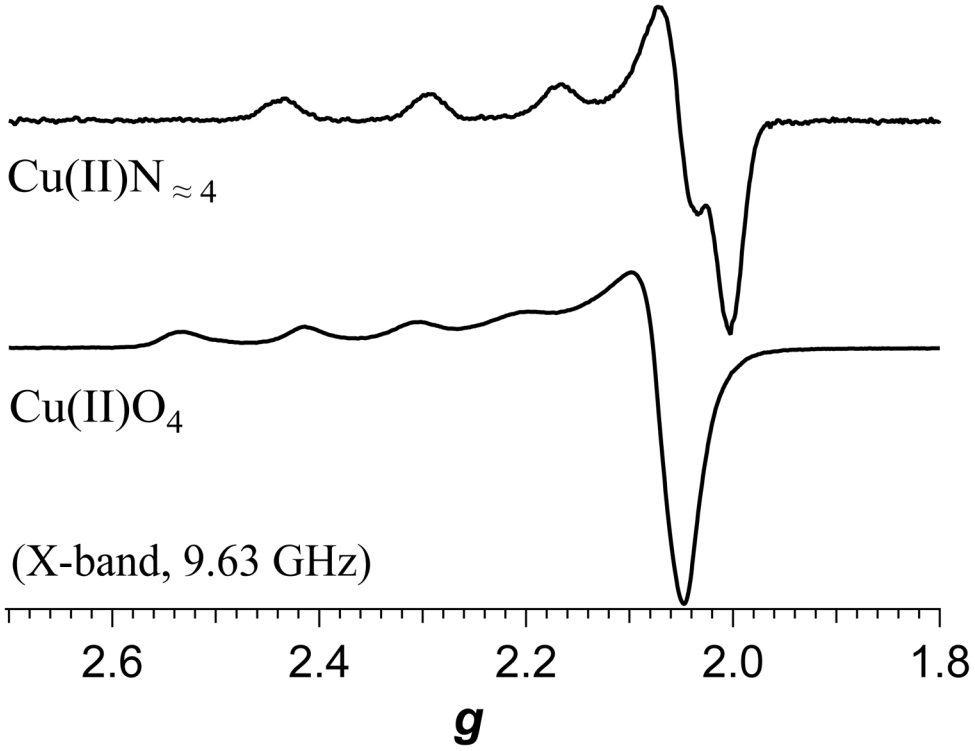


**Figure 1.**
X-band EPR spectra of copper coordinated to α-synuclein (top) and in aqueous solution (bottom).

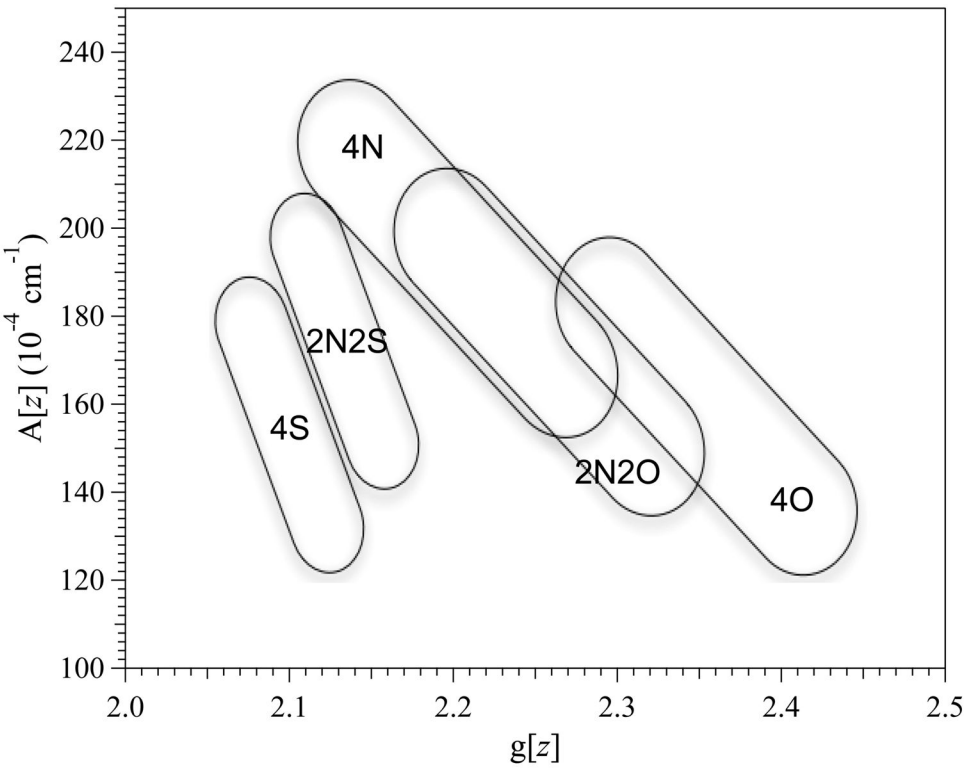


**Figure 2.**

*A*|| versus *g*|| for various copper coordination spheres. Data adapted from ref.{Peisach, 1974 #1510}

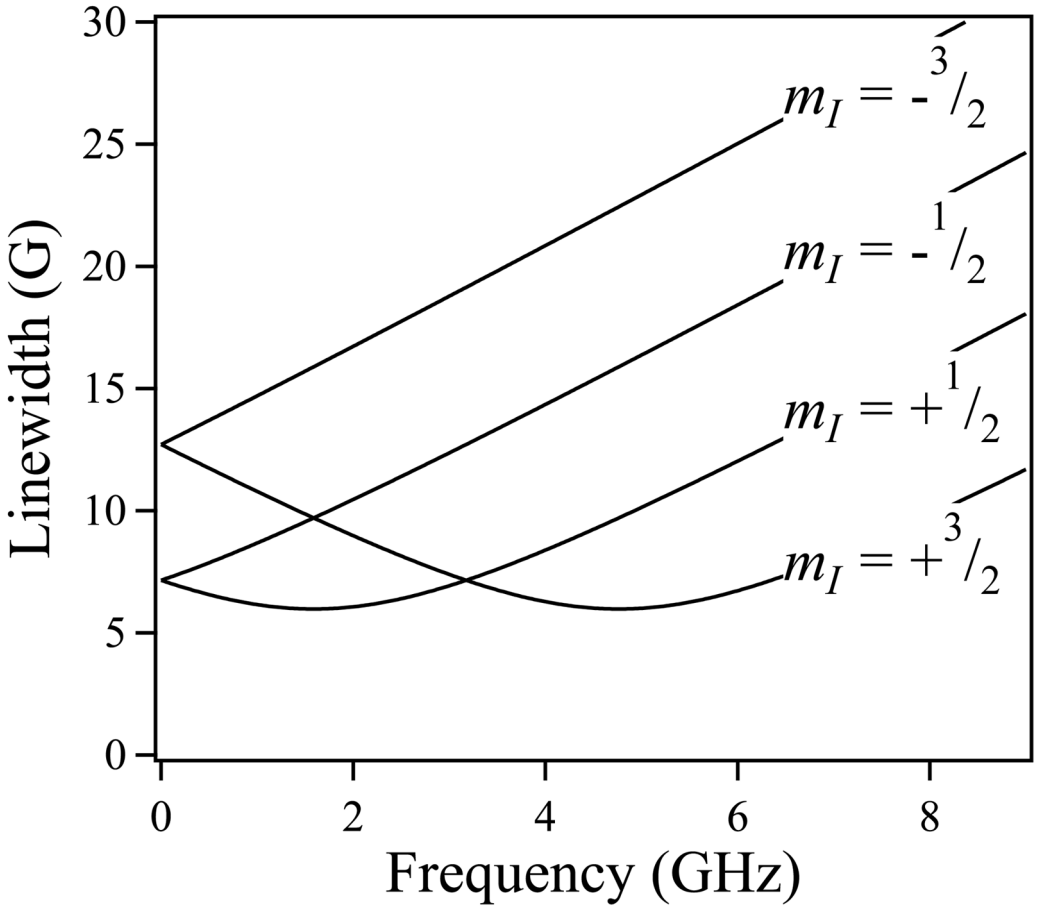


**Figure 3.**
Frequency dependence of strain-dependent line widths in Cu(II) EPR.

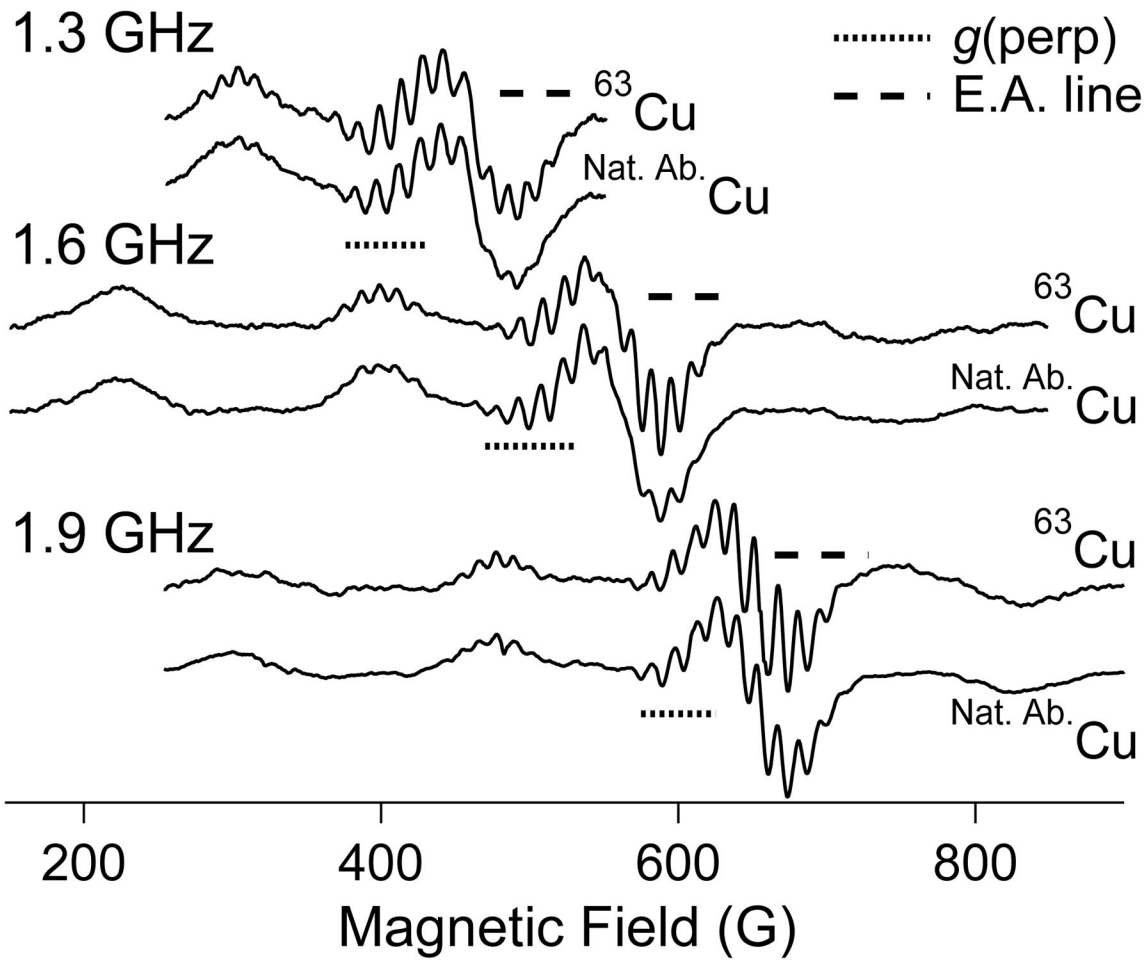


**Figure 4.**

Low-frequency EPR of $^{63}$Cu(II) and naturally abundant Cu(II). The dotted lines highlight the $g\perp$ regions of the spectra and the dashed lines highlight the “extra absorption” or “overshoot” regions.

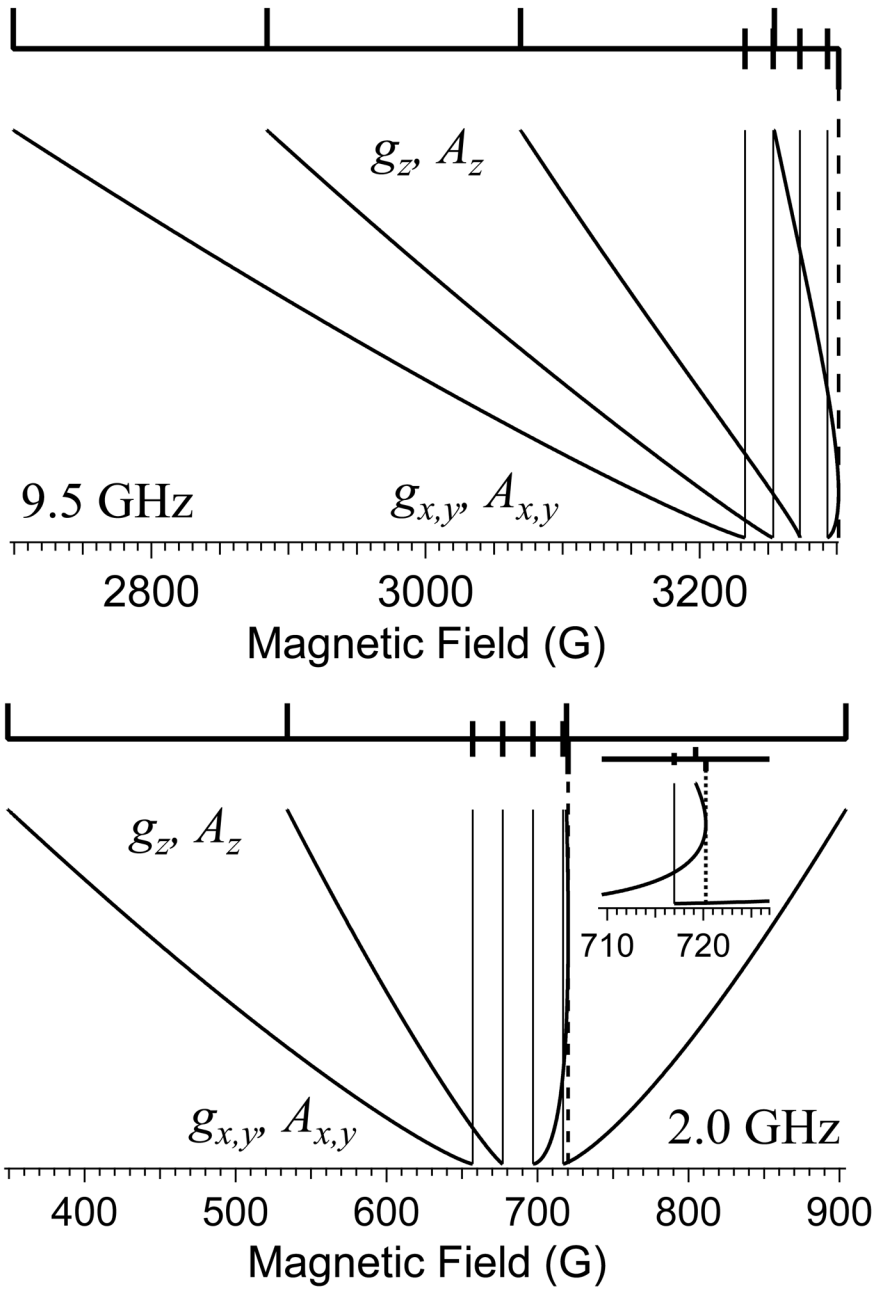


**Figure 5.**
Schematic of the origin of the “extra absorption” or “overshoot” line at X- (top) and L- (bottom) bands.

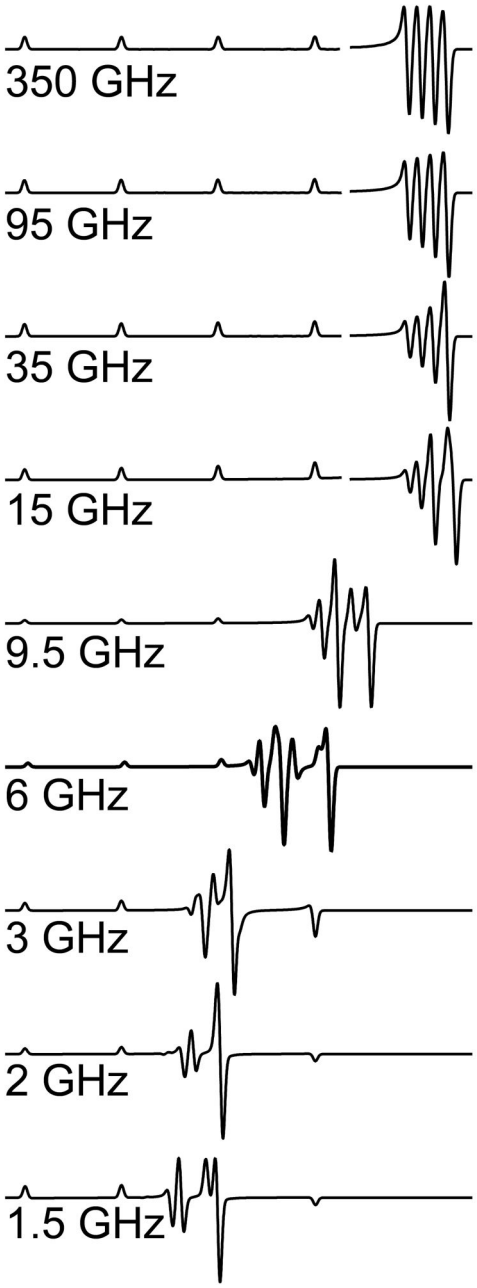


**Figure 6.**
Frequency-dependence of the effect of the overshoot line on the EPR spectra of Cu(II) from 1.5 to 350 GHz.

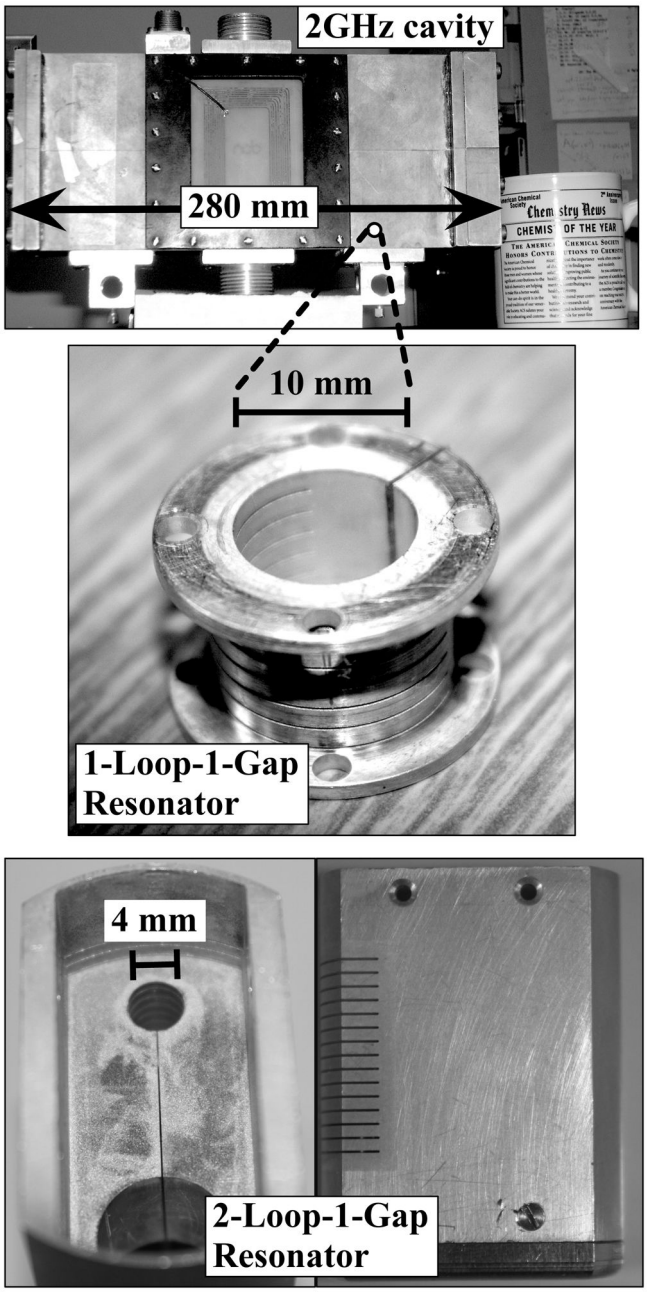


**Figure 7.**

Resonant microwave structures at L-band. Top, resonant cavity. Middle, 1-loop-1-gap 0.5 mL loop-gap resonator. Bottom, 2-loop-1-gap 0.25 mL loop-gap resonator.

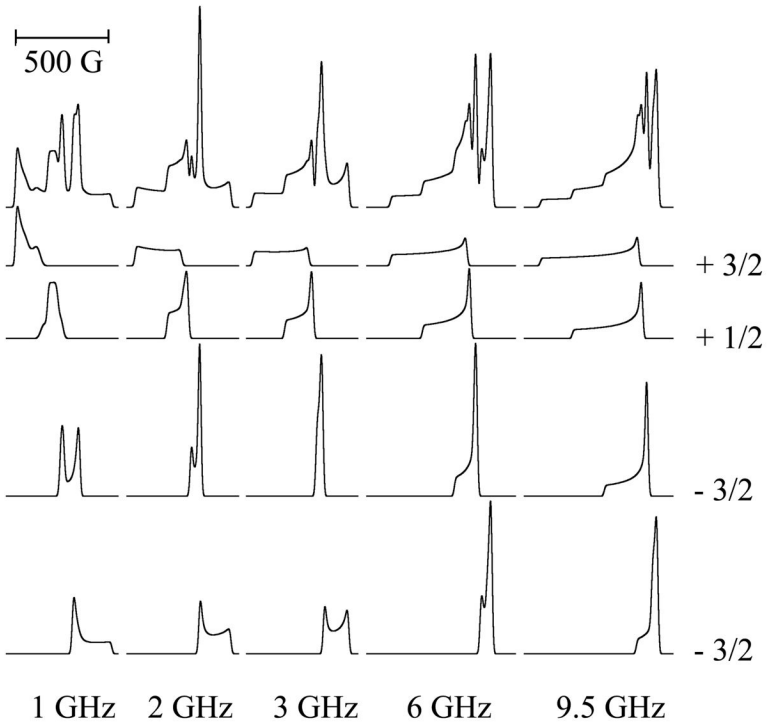


**Figure 8.**
Calculated absorption spectra of Cu(II) and their hyperfine manifolds at various frequencies.

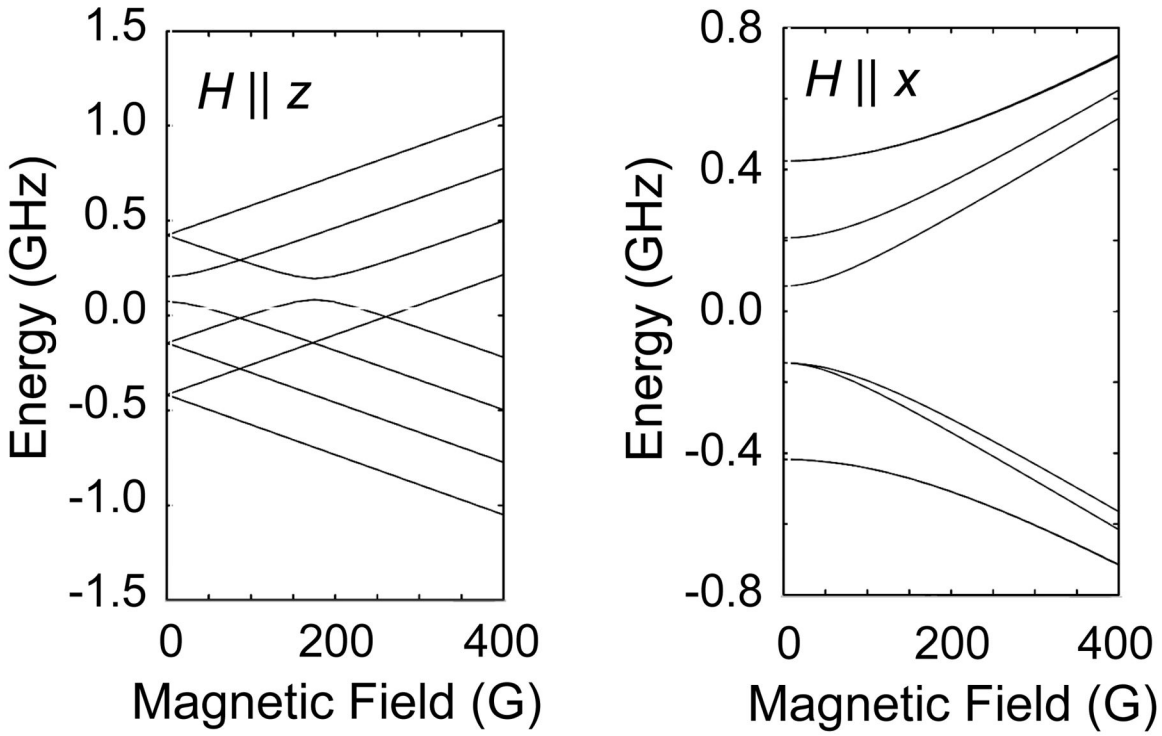


**Figure 9.**
Energy levels of Cu(II) at low resonant magnetic fields.

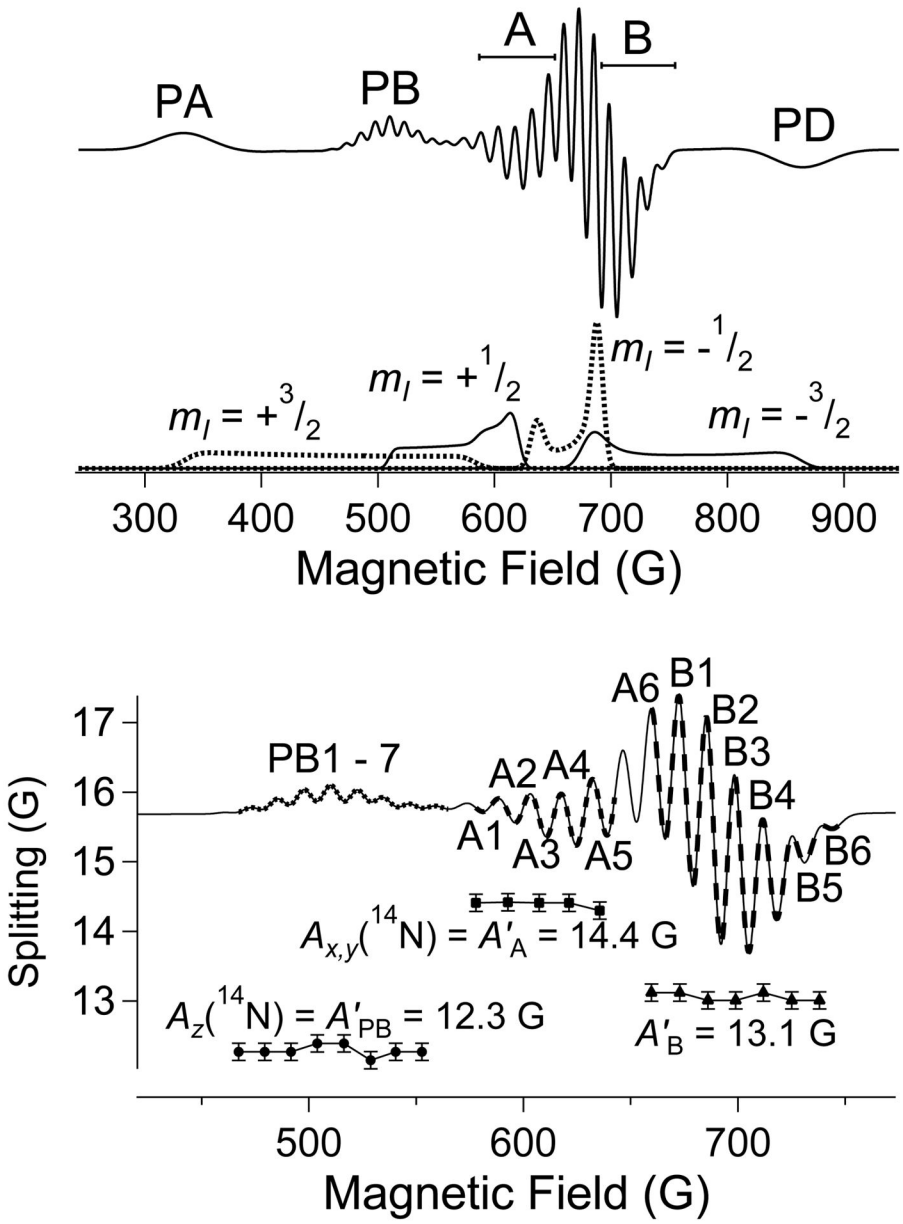


**Figure 10.**
The anatomy of a typical L-band EPR spectrum of nitrogen-coordinated Cu(II).

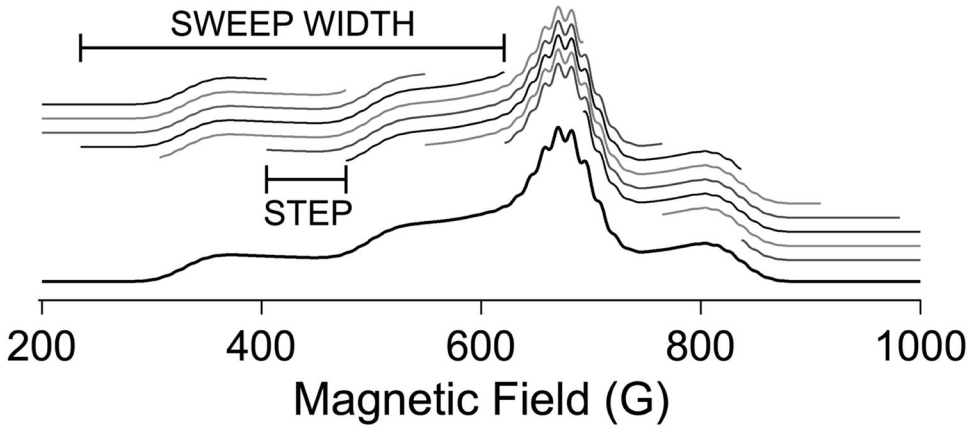


**Figure 11.**

Schematic of the collection of NARS EPR data on Cu(II). In practice, the sweep widths are much smaller than shown here, *e.g.* 5 G.